https://doi.org/10.5194/egusphere-2026-1151
Preprint. Discussion started: 18 March 2026

Dominance of Obliquity over Precession in Polar Temperature Variability: Insights from an Energy Balance Model

Daniel F. J. Gunning[1], Kerim H. Nisancioglu[1], Emilie Capron[2], and Roderik S. W. van de Wal[3,4,5]

[1]Department of Earth Science, University of Bergen and Bjerknes Centre for Climate Research, Bergen, Norway
[2]Université Grenoble Alpes, CNRS, INRAE, IRD, Grenoble INP, IGE, 38000 Grenoble, France
[3]Institute for Marine and Atmospheric research Utrecht, Utrecht University, Utrecht, the Netherlands
[4]Department of Physical Geography, Faculty of Geosciences, Utrecht University, Utrecht, the Netherlands
[5]Royal Netherlands Meteorological Institute (KNMI), De Bilt, the Netherlands

Correspondence: Daniel F. J. Gunning (daniel.gunning@uib.no)

Abstract. The sensitivity of a **Z**onally Averaged **E**nergy and **M**oisture **BA**lance Climate Model **(ZEMBA)** to changes in the Earth's orbit is investigated. The model is intended to explore the dynamics of Quaternary glacial-interglacial cycles, particularly the dominance of 41-kyr obliquity cycles in ice volume and ocean temperature during the Early Pleistocene, despite summer insolation being primarily influenced by 19- and 23-kyr precession cycles. Through equilibrium simulations for the Pre-Industrial and Last Interglacial Period, we demonstrate that ZEMBA's response to strong orbital forcing qualitatively matches the behavior of climate models from the Coupled Model Intercomparison Project Phase 6 (CMIP6). Transient simulations of ZEMBA over the Early Pleistocene reveal a pronounced 41-kyr cyclicity in surface temperatures at the polar latitudes, in correspondence to variations in the Earth's obliquity. Sensitivity experiments underscore the essential role of sea ice in driving temperature variability in the polar regions. The dominant 41-kyr cyclicity in surface air temperature is attributed to obliquity's influence on winter sea ice extent, which governs the release of substantial ocean heat to the atmosphere. The more subdued effect of precession on surface air temperature is linked to the counterbalancing relationship between insolation intensity and summertime duration, which constrains variability in both winter sea ice and ocean heat fluxes.

1 Introduction

Beginning around 2.58 million years before present (Ma), the Quaternary is a period of pronounced variability in Earth's climate history owing to the cyclic expansion and retreat of ice sheets over North America and northern Europe. Known as glacial-interglacial cycles, these fluctuation in ice volume and sea level (Elderfield et al., 2012; Rohling et al., 2014) are accompanied by changes in surface temperature (Jouzel et al., 2007) and atmospheric CO_2 levels (Bereiter et al., 2015). Sediment cores recovered from the deep-sea provide an important source of information on these glacial-interglacial cycles. The $\delta^{18}O$ of fossilized micro-organisms known as foraminifera contain valuable information on past variability in both global ice volume and the temperature of the oceans (Lisiecki and Raymo, 2005; Ahn et al., 2017). These proxy records show the dominant periodicity of the glacial-interglacial cycles was ∼100 thousand years (-kyr) over the last 1 Ma accompanied by smaller 41-kyr and 23-kyr cycles. Yet prior to the Mid-Pleistocene Transition (Clark et al., 2006; Berends et al., 2021) during

https://doi.org/10.5194/egusphere-2026-1151
Preprint. Discussion started: 18 March 2026

the Early Pleistocene, ice volume and ocean temperature varied on regular 41-kyr cycles (Fig. 1a-b). In a previous study, we introduced a **Z**onally Averaged **E**nergy and **M**oisture **BA**lance Climate Model **(ZEMBA)** as a simple, computationally efficient tool for studies of the glacial-interglacial cycles (Gunning et al., 2025). Here, we document the sensitivity of ZEMBA to changes in the Earth's orbit around the Sun, which is widely acknowledged to be the 'pacemaker' of Quaternary climate variability (Hays et al., 1976).

In canonical Milanković theory, changes in the Earth's obliquity and climatic precession pace the growth and decay of Northern Hemisphere (NH) ice sheets by controlling summer insolation at the high northern latitudes. Obliquity describes the tilt of the Earth's rotational axis (varying on a regular 41-kyr cycle) and climatic precession (hereafter 'precession') determines at what time of year the Earth is closest to the Sun (varying on a main 23- and weaker 19-kyr cycle). According to Milanković, milder NH summers–driven by a lower obliquity and a greater distance between the Earth and the Sun–enables snow and ice to persist from one winter to the next, which aided by positive snow-albedo feedbacks can develop into full glacial conditions. While the ∼100-kyr cycles of the Late Pleistocene are not an expected outcome of Milanković theory, statistical studies indicate the timing of deglaciations is controlled by the combined effect of obliquity, precession and ice sheet size (Huybers, 2011; Parrenin and Paillard, 2012; Tzedakis et al., 2017; Hobart et al., 2023). Moreover, modelling studies suggest that precession, and its amplitude modulation by the eccentricity cycle, is important for generating the ∼100-kyr cyclicity (Ganopolski and Calov, 2011; Abe-Ouchi et al., 2013). Yet despite evidence for the combined influence of precession and obliquity in the Late Pleistocene, the glacial-interglacial cycles of the Early Pleistocene appear to be dominated by the 41-kyr obliquity cycle, with little explained variance on precession timescales.

To illustrate the '41-kyr problem' (Raymo and Nisancioglu, 2003), we show changes in $\delta^{18}O$ during the Early Pleistocene (Fig. 1a-b) as compared to summer insolation (Fig. 1e-i). As precession is the primary control of peak summer insolation intensity, it is strongly reflected in most metrics of summer insolation. For example, most variance in summer solstice insolation is concentrated at the precession frequency (Fig. 1f-g). Moreover, the 'summer caloric half-year' metric used by Milanković contains near-equal contributions of obliquity and precession to its variance at 65°N (Fig. 1h-i). Given summer insolation is predicted to be crucial for triggering the waxing and waning of NH ice sheets, we might therefore expect the 19- and 23-kyr (averaging to ∼21-kyr) cycles of precession to be strongly reflected in our proxies of the glacial-interglacial cycles. Yet the benthic $\delta^{18}O$ proxy for ice volume and ocean temperature varies predominantly at the 41-kyr obliquity cycle (Fig. 1b). This conundrum is known as the '41-kyr problem'.

One mechanism used to resolve the 41-kyr problem involves an anti-correlation between summer insolation intensity and summertime duration at the precession timescale (Huybers, 2006). This counterbalancing is related to Kepler's second law, which dictates when the Earth reaches its closest distance to the Sun (and insolation intensity is highest), angular velocity is highest (and thereby summertime duration becomes shorter). Therefore, when insolation is integrated above a threshold (e.g. 275 W m^2) separating days above and below 0°C- known as integrated summer insolation (ISI)- the ∼21-kyr precession cycle can be significantly diminished (Fig. 1j-k), in correspondence to the $\delta^{18}O$ record. As opposed to insolation for one day of year (i.e. the summer solstice), ISI is considered to be more representative for the ablation of NH ice sheets over the duration of melt season. The ISI metric is sensitive to the choice of threshold, however, with a higher threshold (synonymous with a

https://doi.org/10.5194/egusphere-2026-1151
Preprint. Discussion started: 18 March 2026

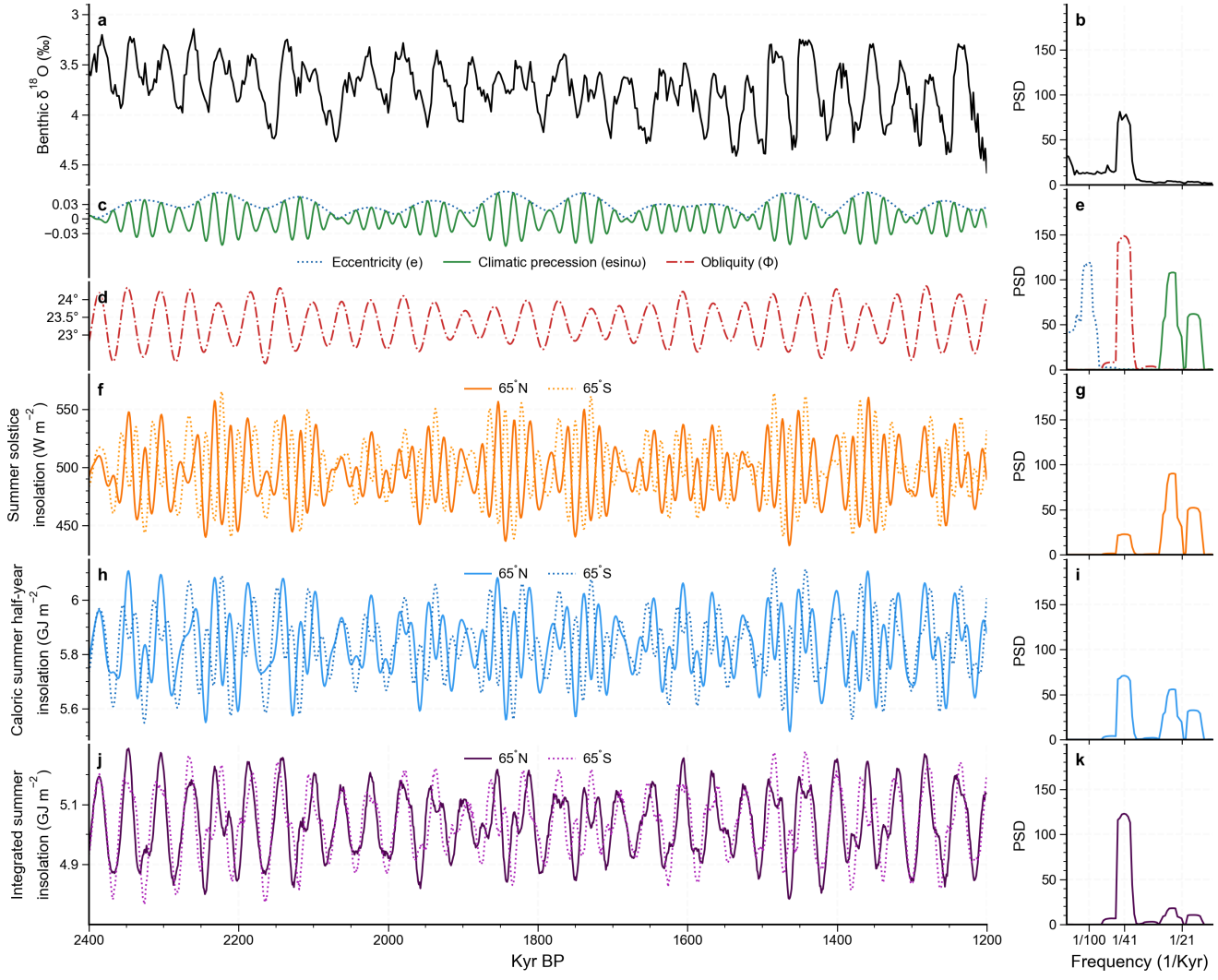

Figure 1. Variations from 2.4 to 1.2 Ma in: (a-b) the benthic δ^{18}O stack from Ahn et al. (2017); (c-e) eccentricity, climatic precession and obliquity according to the Laskar et al. (2004) solution; (f-g) daily mean summer solstice insolation at 65°N on 21st June and 65°S on 21st December; (h-i) caloric summer half-year insolation at 65°N and 65°S; and (j-k) integrated summer insolation above a threshold of 275 W m^{-2} at 65°N and 65°S. Shown is both the time-series (a,c,d,f,h,j) and the power spectral density (PSD) of the time-series (b,e,g,i,k). In this and all subsequent figures, the PSD is calculated using the multi-taper method from the Pyleoclim python package (Khider et al., 2022) with a time-bandwidth product of 4.

https://doi.org/10.5194/egusphere-2026-1151
Preprint. Discussion started: 18 March 2026

colder background climate state) containing stronger variance at the precession period. Moreover, the relative contributions of obliquity and precession variance to any summer insolation metric is sensitive to the latitude, with obliquity having a greater effect over the higher latitudes, and precession exerting a stronger influence at the lower latitudes. While the relative contributions of precession and obliquity to summer insolation variance is sensitive to both the metric and the latitude, they still contain a stronger precession signal than observed in the benthic $\delta^{18}O$ stack for the Early Pleistocene (Raymo and Lisiecki, 2005; Ahn et al., 2017). Moreover, several model simulations of the NH ice sheets during the Early Pleistocene generate a stronger precession cycle than observed in proxy records (Berger et al., 1999; Willeit et al., 2019; Watanabe et al., 2023).

Another mechanism used to resolve the 41-kyr problem involves a cancellation of ~21-kyr cycles between the NH ice sheets and Antarctica. Intrinsic to this hypothesis is that the precession forcing is equal and opposite between the NH and the Southern Hemisphere (SH), such that when NH summers align with the Earth's closest pass to the Sun, SH summers coincide with the furthest Earth-Sun distance (Fig. 1f). Therefore, Raymo et al. (2006) put forward that ice sheets in both hemispheres may have varied with local summer insolation, which can cancel each other out (at the precession frequency) in globally averaged proxies of ice volume, such as the benthic $\delta^{18}O$ record (Morée et al., 2021). Given Antarctica is more isotopically depleted (i.e. a larger mean $\delta^{18}O$) compared to the NH ice sheets, relatively small variations of Antarctica could offset larger ice volume fluctuations in the north. However, conditional to the 'anti-phased hypothesis' is that the Early Pleistocene was warmer than present, with land-terminating margins around Antarctica which are sensitive to local summer insolation, unlike the present day. It remains unclear whether a climate regime exists with both large NH ice sheets and partly deglaciated margins around Antarctica, that balance each other out in the benthic $\delta^{18}O$ record. To our knowledge, the possibility of Antarctica and the NH ice sheets varying out-of-phase from one another has not been investigated with anything other than a conceptual model, where ice volume is made a linear function of local summer insolation (Raymo et al., 2006).

In this study, we perform simulations of ZEMBA in response to changing orbital parameters. In the context of the '41-kyr problem' and the mechanisms proposed to resolve it, we investigate the relative importance of obliquity and precession in driving variability in the model. First, we perform equilibrium simulations of ZEMBA for the Pre-Industrial (PI) and Last Interglacial Period (LIG) (Section 4.1). These two interglacials represent times of similar CO_2 levels and ice sheet distributions but with a different orbital configuration, which has been utilized to investigate the sensitivity of state-of-the-art climate models to changes in the Earth's orbit, serving as a useful point of comparison to ZEMBA. Next, we perform a transient simulations of the model over the Early Pleistocene from 2.4 to 1.2 Ma (Section 4.2) and assess the relative importance of obliquity and precession for driving orbital variability within ZEMBA (Section 4.3). Finally, we investigate the importance of albedo feedbacks over land and ocean for amplifying the response to changes in the orbital parameters (Section 4.4). Prior to this, we provide a brief overview of ZEMBA (Section 2) and describe the experimental set-up for the simulations in more detail (Section 3).

https://doi.org/10.5194/egusphere-2026-1151
Preprint. Discussion started: 18 March 2026

2 Model Description

ZEMBA is a **Z**onally averaged **E**nergy and **M**oisture **BA**lance climate model that serves as a computationally efficient tool for studies of Quaternary climate variability (Gunning et al., 2025). Given a seasonal cycle in insolation, an atmospheric CO_2 concentration and a percentage of land and ice sheet cover, ZEMBA calculates the zonal-mean (i.e. east-west averaged) distribution of surface temperature and precipitation. The model comprises an atmospheric layer that overlies a surface divided into land and a six-layered ocean transport model. Atmospheric heat transport is represented as a diffusive process along equator-to-pole gradients in moist static energy at the surface. The ocean model includes both a prescribed advective (overturning) and a diffusive (eddy/gyre) component of heat transport. Once the temperature of the surface ocean layer drops below the freezing point of sea-water, sea ice of a prescribed thickness is allowed to form. Should sea ice expand to fill an entire latitudinal zone, the temperature of sea ice drops below zero, while the surface ocean layer remains at freezing point. The inclusion of a moisture balance equation enables the simulation of precipitation and snowfall. A Hadley cell parameterization produces an equatorward flux of latent energy at the tropics, thereby achieving a realistic representation of the hydrological cycle. The competition between snow accumulation (via the hydrological cycle) and surface melting (via the surface energy balance) determines snow coverage over land, where the snow albedo is made a function of surface air temperature. ZEMBA is simulated at a 5° resolution. A mixed ocean layer is assumed to cover the entire surface from 80° - 90°N and land occupies everywhere poleward of 75°S.

Previously, we demonstrated that ZEMBA can approximate zonal-mean climate variables including surface temperature, precipitation, sea ice, radiative fluxes and meridional heat transport in correspondence to both global climate models (GCMs) and observations for the PI period. Moreover, a simulation of ZEMBA using Last Glacial Maximum (LGM) boundary conditions captures the zonal-mean anomalies in temperature and precipitation, relative to the PI, in broad agreement with GCMs and reconstructions. The global and annual mean warming in response to a doubling of atmospheric CO_2 (3.6°C) is also consistent with climate models of higher complexity, and the polar amplification of warming which is most intense over the NH and during the winter months, is in qualitative agreement to both GCMs and observations. A detailed description of ZEMBA, including equilibrium simulations for the PI, LGM and a doubling of atmospheric CO_2 levels, is provided in Gunning et al. (2025). Here, we address the sensitivity of the model to changes in the Earth's orbital configuration with a focus on the 41-kyr problem. The model parameters used for tuning ZEMBA to the PI (Gunning et al., 2025) are maintained in this study. The percentage of land, ocean and ice sheet cover for each latitudinal band is kept fixed in all experiments, and is taken from the ICE-6G_C dataset for the present-day (Argus et al., 2014; Peltier et al., 2014).

3 Experimental Setup

To constrain ZEMBA's sensitivity to changing orbital parameters relative to state-of-the-art climate models, we first conduct equilibrium simulations of the model for the PI (E_{PI}) and Last Interglacial Period (E_{LIG}). The Last Interglacial Period (LIG) at 127 ka represents a time period when atmospheric CO_2 levels and the distribution of ice sheets were similar to the PI, but the orbital configuration was marked by higher eccentricity, greater obliquity, and NH summers occurring near perihelion. Conse-

https://doi.org/10.5194/egusphere-2026-1151
Preprint. Discussion started: 18 March 2026

Table 1. Model experiments, orbital forcing and boundary conditions. In all experiments the percentage of land and ice sheet cover for each latitude band is kept fixed at the PI. Equilibrium simulations are run for 3,000 years. Transient simulations are run from 2.45 to 1.2 Ma

	Obliquity (°)	Precession (°)	Eccentricity	Sea Ice	Snow Cover	CO_2 (ppm)
Equilibrium simulations						
E_{PI}	23.459	100.33	0.016764	varying	varying	284
E_{LIG}	24.040	275.41	0.039378	varying	varying	275
Transient simulations						
T_{BE}	varying	varying	varying	varying	varying	284
T_{FX_PR}	varying	Fixed: E_{PI}	Fixed: E_{PI}	varying	varying	284
T_{FX_OB}	Fixed: E_{PI}	varying	varying	varying	varying	284
T_{FX_SI}	varying	varying	varying	Fixed: E_{PI}	varying	284
T_{FX_SC}	varying	varying	varying	varying	Fixed: E_{PI}	284
T_{FX_SIC}	varying	varying	varying	Fixed: E_{PI}	Fixed: E_{PI}	284

quently, the LIG has been recognized as a key period in the recent geological record for studying climate change driven almost exclusively by orbital variations (Otto-Bliesner et al., 2017). It has therefore been included as one of the Tier 1 simulations in the Coupled Model Intercomparison Project (CMIP6) and the Paleoclimate Modeling Intercomparison Project (PMIP4). The differences in climate relative to the PI have been analyzed across an ensemble of 17 climate models participating in the *lig127k* experiment (Otto-Bliesner et al., 2021; Kageyama et al., 2021), providing a useful basis for assessing ZEMBA's orbital sensitivity. The exact orbital configuration and CO_2 concentration used for the EQ_{PI} and EQ_{LIG} experiments matches the boundary conditions used in the PMIP4 *lig127k* ensemble (Otto-Bliesner et al., 2017), as detailed in Table 1.

Next, we explore ZEMBA's transient sensitivity to changing orbital parameters by performing a simulation spanning 2.45 to 1.2 Ma. The orbital parameter variations are based on the solution by Laskar et al. (2004) and updated at 1-kyr intervals. The initial 50-kyr period, representing the model's spin-up, is excluded from the analysis. In the baseline orbital experiment (T_{BE}), the model is driven by variations in all three orbital parameters. To further investigate the individual contributions of obliquity and climatic precession to climate variability in T_{BE}, two additional simulations are performed: one where only obliquity varies (T_{FX_PR}), and another where only climatic precession varies (T_{FX_OB}), with the other orbital parameter(s) fixed to their present-day values. A summary of the experimental setup is provided in Table 1.

Finally, to assess the role of albedo feedbacks over land and ocean in amplifying the response to orbital forcing within ZEMBA, we conduct an additional set of experiment. In these experiments, either sea ice (T_{FX_SI}), snow cover (T_{FX_SC}) or both (T_{FX_SIC}) are fixed to the seasonal cycle from the E_{PI} simulation. In the T_{FX_SI} experiment, both the seasonal cycle of sea ice cover and sea ice temperature are prescribed from the E_{PI} simulation. Similarly, in the T_{FX_SC} experiment, the seasonal cycle of snow cover over land is prescribed from E_{PI}.

https://doi.org/10.5194/egusphere-2026-1151
Preprint. Discussion started: 18 March 2026

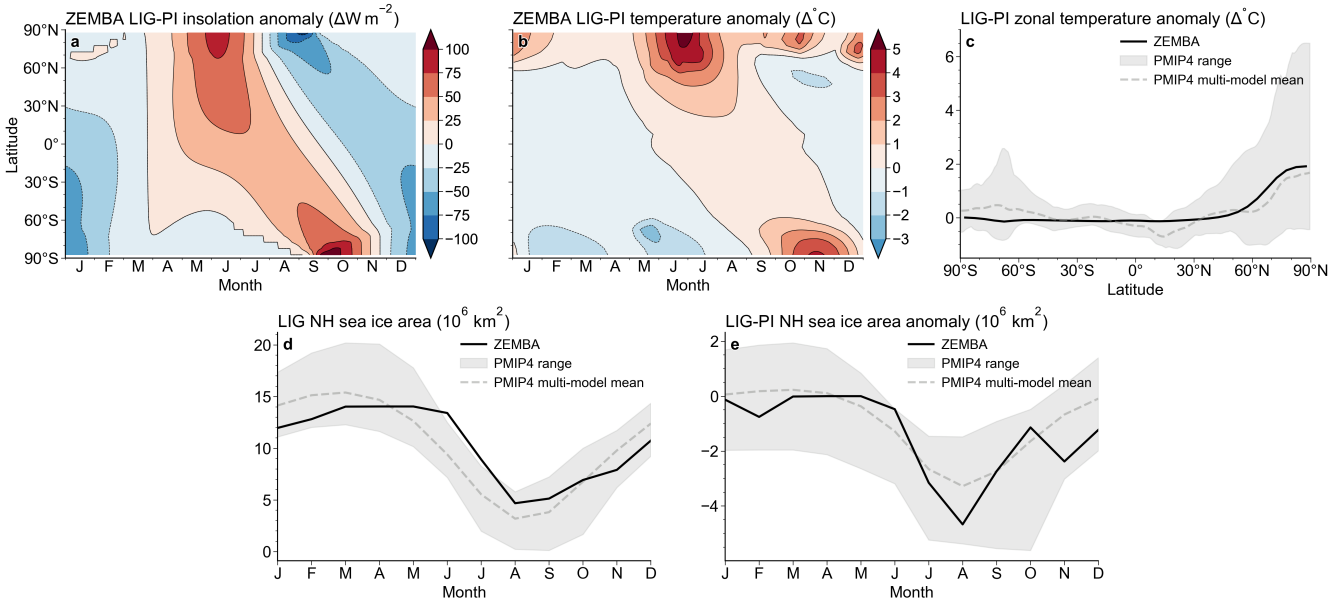

Figure 2. (a-b) The Last Interglacial Period minus Pre-Industrial (LIG-PI) anomalies in the latitudinal and seasonal distribution of insolation (a) and surface air temperature (b) for ZEMBA; (c-e) the LIG-PI difference in zonal average and annual mean temperature (c), the LIG seasonal cycle in NH sea ice coverage (d) and the LIG-PI anomalies in NH sea ice coverage (e). Shown is model output from ZEMBA (E_{LIG}-E_{PI}: black line) compared to the *lig127k* multi-model PMIP4 average (gray dashed line) and range (gray region).

4 Results

4.1 Equilibrium simulations for the PI (E_{PI}) and LIG (E_{LIG})

Figure 2a shows the difference in the seasonal and latitudinal distribution of insolation received between the E_{LIG} and E_{PI} experiments. Overall, the NH receive more insolation during early summer, and less during early winter, for the LIG relative to the PI. The insolation differences are most pronounced at the higher latitudes, with large positive anomaly exceeding 75 W m^{-2} during June, and large negative anomalies exceeding -50 W m^{-2} during September. For the SH, conversely, the LIG receives more insolation during the winter, and less during the summer, relative to the PI. At the high latitudes, the SH can receive 50 W m^{-2} more insolation during September-October, and 50 W m^{-2} less insolation during December-January.

Figure 2b shows the corresponding changes in surface temperature between the E_{LIG} and E_{PI} experiments, driven by differences in the orbital configuration. For the NH, the lower and mid-latitudes become warmer during summers, and colder during winters, reflecting the differences in insolation. For latitudes poleward of 60°N, however, the LIG warming is persistent throughout the year, and can exceed 5°C during the summer months. Conversely, for the polar latitudes of the SH, the LIG warming is intense during September-December, but is cooler than the PI for the rest of the year. For changes in zonal average, annual mean temperature relative to the PI (Fig 2c), there is a good correspondence between ZEMBA and the multi-model

https://doi.org/10.5194/egusphere-2026-1151
Preprint. Discussion started: 18 March 2026

mean from the *lig127k* ensemble. In particular, ZEMBA simulates an annual mean warming in the NH polar regions (60-90°N) of 1.24°C, which is slightly greater than the 0.82±1.20°C of warming captured in the *lig127k* ensemble, but still within uncertainty. However, Figure 2c also demonstrates the large spread of temperature change in the NH polar regions for the *lig127k* ensemble, ranging from -0.39 to 3.88°C (Otto-Bleisner et al., 2021). For the SH polar regions, ZEMBA simulates a negligible change in temperature of -0.01°C, in broad agreement with the multi-model mean of 0.38±0.63°C for *lig127k*, although only 3 of the 17 models that contributed to the ensemble simulated an annual mean cooling for the SH polar regions (Otto-Bleisner et al., 2021). Finally, the change in global mean temperature for the LIG is 0.02°C, compared to -0.02±0.32°C for *lig127k* (Otto-Bleisner et al., 2021).

Figure 2d shows the seasonal cycle for NH sea ice cover in E_{LIG}, while Figure 2e shows its difference relative to E_{PI}. The seasonal cycle of sea ice corresponds reasonably well between ZEMBA and the *lig127k* ensemble, with ZEMBA capturing the minima in sea ice area that occurs around August-September. However, the timing of maximum sea ice coverage occurs somewhat later for ZEMBA (around May) than *lig127k* (around March), and ZEMBA simulates a sea ice area that slightly exceeds the upper range of the *lig127k* ensemble from the months of June to July. Relative to the pre-industrial period, both ZEMBA and *lig127k* capture the pronounced reduction in sea ice cover during the summer months, with the largest reduction in August-September resulting in an enhanced seasonal cycle of Arctic sea ice for the LIG.

Since ZEMBA's primary goal is to investigate the climate's sensitivity to changes in Earth's orbital configuration, and to explore the relative contributions of obliquity and precession, the strong alignment between ZEMBA and the PMIP4 *lig127k* ensemble in terms of orbitally driven changes in temperature and sea ice is particularly encouraging. This is especially notable given that ZEMBA has been tuned to the PI and does not account for short-term climate feedbacks related to vegetation, clouds, and dust. Moreover, ZEMBA's simplicity facilitates a detailed analysis of the processes driving the observed changes, including multiple sensitivity experiments that can disentangle the relative importance of different orbital parameters (e.g., obliquity and precession) and feedbacks (e.g., sea ice and snow cover) in driving variability in the model. In the following section, we explore the transient sensitivity of the model to the full range of orbital parameters and assess the role of obliquity and precession.

4.2 Baseline transient simulation (T_{BE})

The response of ZEMBA to variations in all three orbital parameters (T_{BE}) is shown in Figure 3 for the NH polar regions (60° - 90°N). Changes in surface air, land and ocean temperatures are tightly coupled, with temperature maxima occurring during periods of above-average obliquity (as indicated by grey bands). Notably, 75% of the variance in surface air temperature is concentrated in the obliquity band (1/41 kyr ± 1/100 kyr), compared to only 21% in the precession band (1/21 kyr ± 1/100 kyr) (Fig. 4a). Warmer temperatures are associated with reductions in the extent of both sea ice and snow cover, but unlike surface temperatures, changes in sea ice and snow cover exhibit strong variance in both the obliquity and precession bands. Precipitation and snowfall are inversely correlated, with warmer temperatures resulting in more precipitation and less snowfall, and colder temperatures generating less precipitation but more snowfall. Similar to sea ice and snow cover, changes in precipitation and snowfall contain strong variance in both the obliquity and precession bands. The transport of atmospheric heat (AHT) within ZEMBA is controlled by the equator-to-pole gradient in moist static energy (MSE). As temperatures rise in

https://doi.org/10.5194/egusphere-2026-1151
Preprint. Discussion started: 18 March 2026

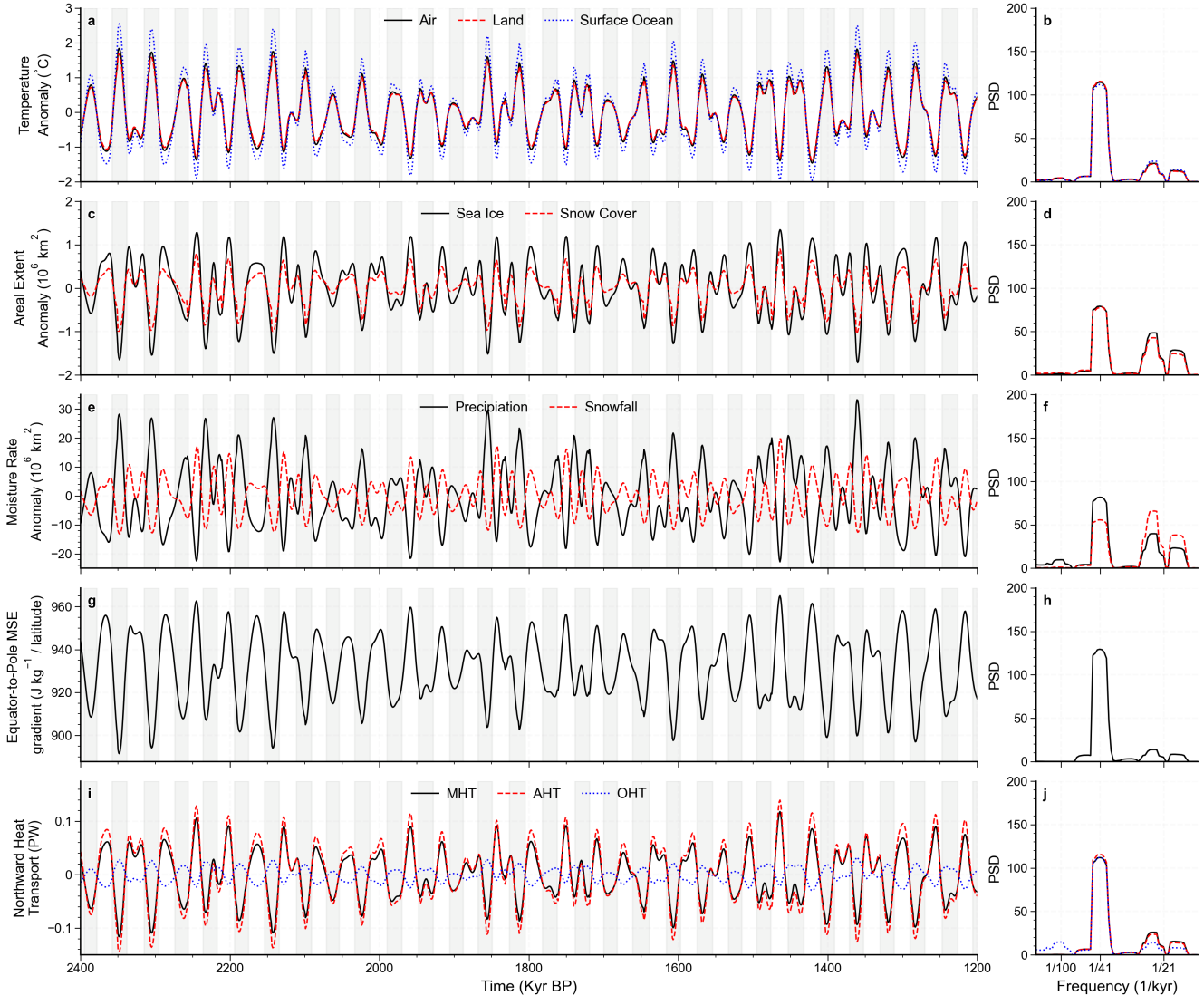

Figure 3. For the baseline orbital experiment (T_{BE}), where all orbital parameters are varying, changes in the following variables are shown: surface air, land, and ocean temperatures (a-b); sea ice and snow cover area (c-d); and precipitation and snowfall (e-f), all averaged between 60° to 90°N. Additionally, the equator-to-pole gradient in moist static energy (MSE), with the equator averaged from 0°-30°N and the pole from 60°-90°N (g-h). Changes in the northward flux of atmospheric (AHT), oceanic (OHT), and total heat transport (MHT) at 60°N is also illustrated (g-h).

https://doi.org/10.5194/egusphere-2026-1151
Preprint. Discussion started: 18 March 2026

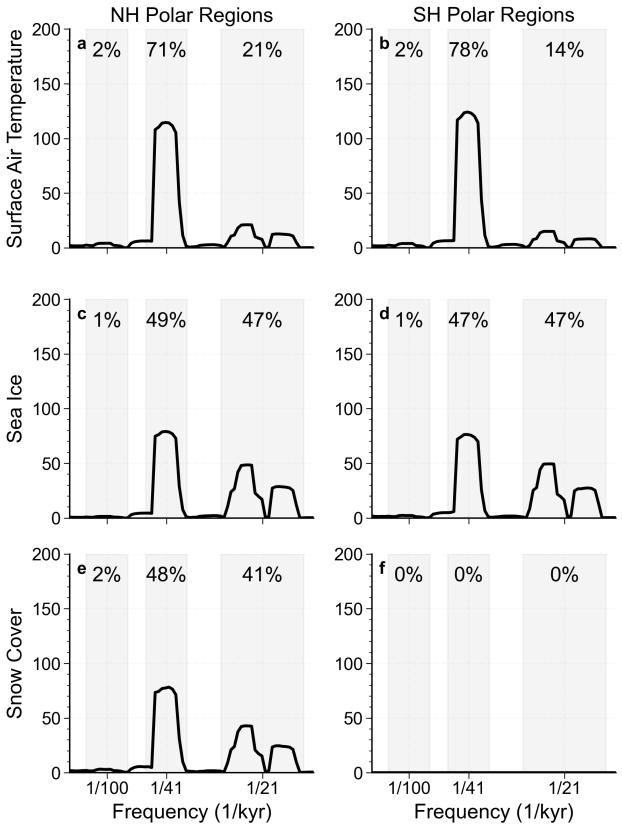

Figure 4. Power spectral density in the NH polar (60°-90°N) and SH polar (60°-90°S) regions for changes in surface air temperature (a-b), sea ice (c-d) and snow cover over land (e-f). Also shown is the percentage of total variance for each variable concentrated at the eccentricity (1/100-kyr ± 1/200-kyr), obliquity (1/41-kyr ± 1/200-kyr) and precession (1/21-kyr ± 1/100-kyr) bands (highlighted in grey).

the NH polar regions, this gradient weakens, resulting in a decrease in AHT at 60°N. Although changes in ocean heat transport (OHT), mainly driven by a constant overturning, slightly offsets any alterations in AHT, the overall changes in total heat transport (MHT) are primarily influenced by AHT. For the SH polar regions (60° - 90°S), changes in surface air temperature contain even more variance at the obliquity band (78%) (Fig. 4b), with warmer temperatures coinciding with reductions in sea ice, increases in both precipitation and snowfall, and decreases in AHT (Fig. S1 in the Supplement).

The influence of changing sea ice and snow cover on surface air temperature is mostly confined to the polar regions. As a result, the global and annual mean surface air temperature fluctuates by no more than 0.43°C, showing distinct cycles of 100- and 41-kyr (Fig. S2 in the Supplement). The 100-kyr cyclicity corresponds to changes in Earth's eccentricity, the sole orbital parameter that affects global and annual mean insolation. This 100-kyr temperature cycle is most pronounced in the mid-latitudes, whereas the 41-kyr cycles are most significant at polar and tropical latitudes, where obliquity has the greatest effect on annual mean insolation (Fig. S3 in the Supplement)

https://doi.org/10.5194/egusphere-2026-1151
Preprint. Discussion started: 18 March 2026

4.3 Fixed precession (T_{FX_PR}) and obliquity (FT_{FX_OB}) simulations

Figure 5 displays the changes in temperature, sea ice and snow cover in the NH polar regions when climatic precession (T_{FX_PR}: red) and obliquity (T_{FX_OB}: green) are held constant. Variations in the Earth's obliquity alone account for the majority of variance in surface air temperature, as evidenced by both the time series (Fig. 5b) and the violin plots (Fig. 5c) comparing the T_{FX_PR} to the T_{BE} experiment. When obliquity is kept fixed, however, and only changes in climatic precession affect the latitudinal and seasonal distribution of insolation, surface temperature variations become more constrained. Indeed, in the T_{FX_OB} experiment, the overall variance in temperature is reduced by almost half as compared to T_{FX_PR}. Only during periods of high eccentricity (represented by yellow shaded sections) does the variability in T_{FX_OB} approach that of the T_{FX_PR} experiment. These fixed orbital experiments further highlight the dominant role of obliquity over precession in controlling surface air temperature in the NH polar regions.

On other hand, changes in either obliquity or precession result in similar variability in NH sea ice (Fig. 5d-e). Over the entire simulation, precession leads to a larger maximum range in sea ice, while obliquity results in a greater standard deviation. During periods of high eccentricity, precession generates more fluctuations in sea ice than obliquity, whereas obliquity dominates when eccentricity is average or below. The near-equal contributions of both obliquity and precession to annual mean sea ice variability is further demonstrated by the strong variance observed in the obliquity and precession bands in the T_{BE} experiment (Fig. 4c). However, variations in either obliquity or precession alone are insufficient to explain the full extent of NH sea ice variability; all three orbital parameters are crucial for driving the complete range of NH sea ice fluctuations.

Similarly, precession drives greater variability in NH snow cover over land, relative to obliquity, during periods of high eccentricity, while obliquity leads to more variability during other periods. Precession appears particularly important in generating strong minima in snow cover extent when eccentricity is high. Once again, the combination of obliquity and precession is essential for capturing the full variability in snow cover, with similar variance present in both bands in the T_{BE} simulation of ZEMBA (Fig. 4e).

Given that precession drives a comparable, if not greater, variability in the annual-mean extent of both NH sea ice and snow cover relative to obliquity, it is unexpected that annual mean surface air temperature in the NH polar regions should be primarily affected by the 41-kyr obliquity cycle. This pattern also holds true for the SH polar regions, where obliquity accounts for the majority of variance in surface air temperature — more so than in the NH — despite both obliquity and precession independently generating a similar variability in annual mean sea ice extent (Fig. S4 in the Supplement).

To better understand ZEMBA's response to variations in obliquity and climatic precession, Figure 6 illustrates the differences in insolation, temperature, ocean heat fluxes (OHFs) and sea ice for extremes in both orbital parameters for the NH polar regions over the whole 1.4 Ma simulation. These extremes are identified by maxima and minima in summer solstice insolation for the T_{FX_PR} (Fig. 6a) and T_{FX_OB} experiments (Fig. 6b), respectively. More specifically, these maxima and minima correspond to the periods of highest and smallest degrees of axial tilt in the T_{FX_PR} experiment, and for NH summers coinciding with the perihelion and aphelion in the T_{FX_OB} experiment. The seasonal cycles in insolation, temperature, OHFs and sea ice are then

https://doi.org/10.5194/egusphere-2026-1151
Preprint. Discussion started: 18 March 2026

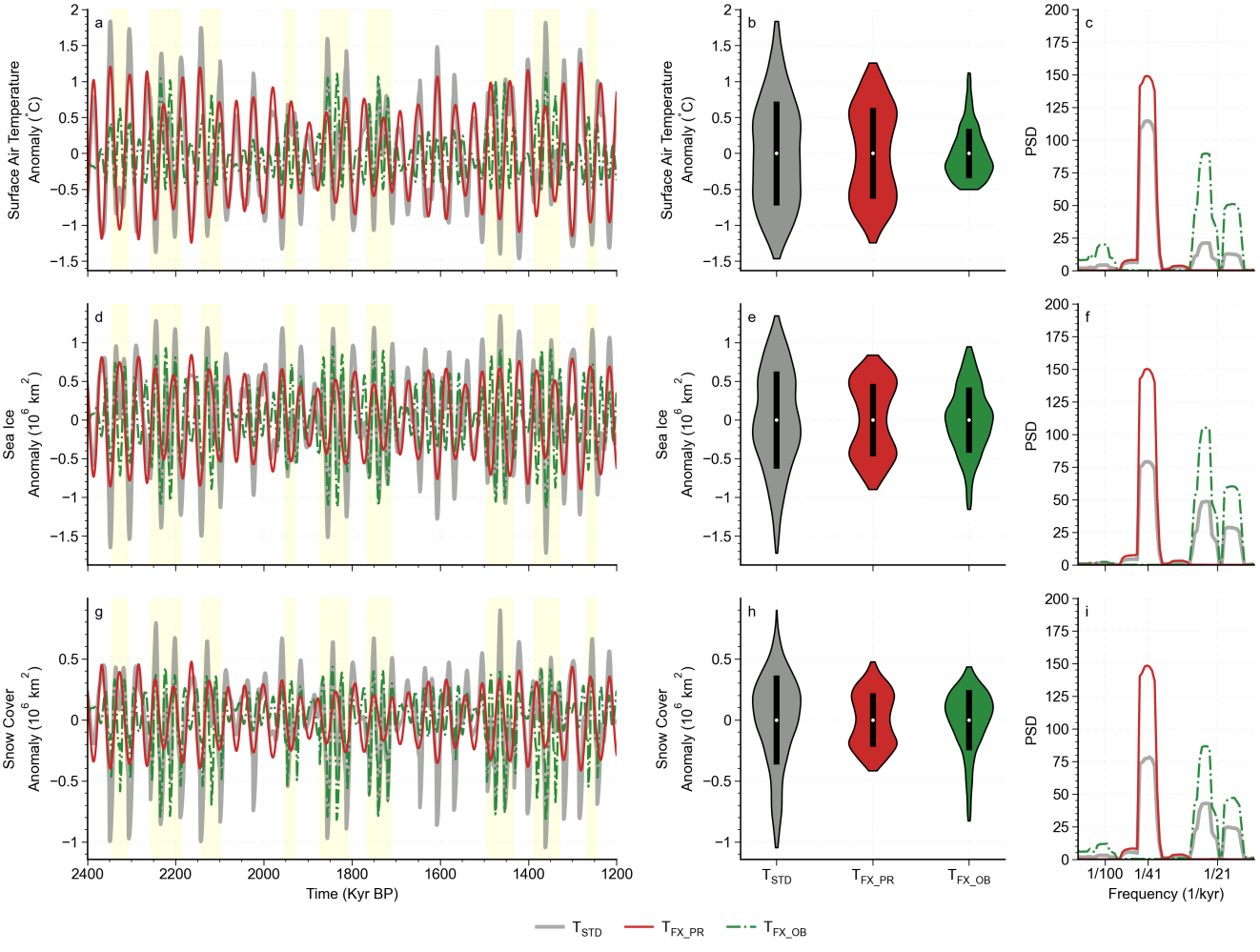

Figure 5. For the standard T_{BE} (in grey), the fixed precession T_{FX_PR} (in red), and the fixed obliquity T_{FX_OBL} (in green) experiments, the top row shows changes in surface air temperature (a-c), the middle row shows sea ice variations (e-f), and the bottom row shows changes in snow cover (g-i), for the NH polar regions (60°-90°N). The figure include the time series (a,d,g), violin plots illustrating the distributions (b,e,h), and the power spectral density (c,f,i) corresponding to each variable. Shaded yellow regions in (a,d,g) represents periods when eccentricity is above 0.035.

https://doi.org/10.5194/egusphere-2026-1151
Preprint. Discussion started: 18 March 2026

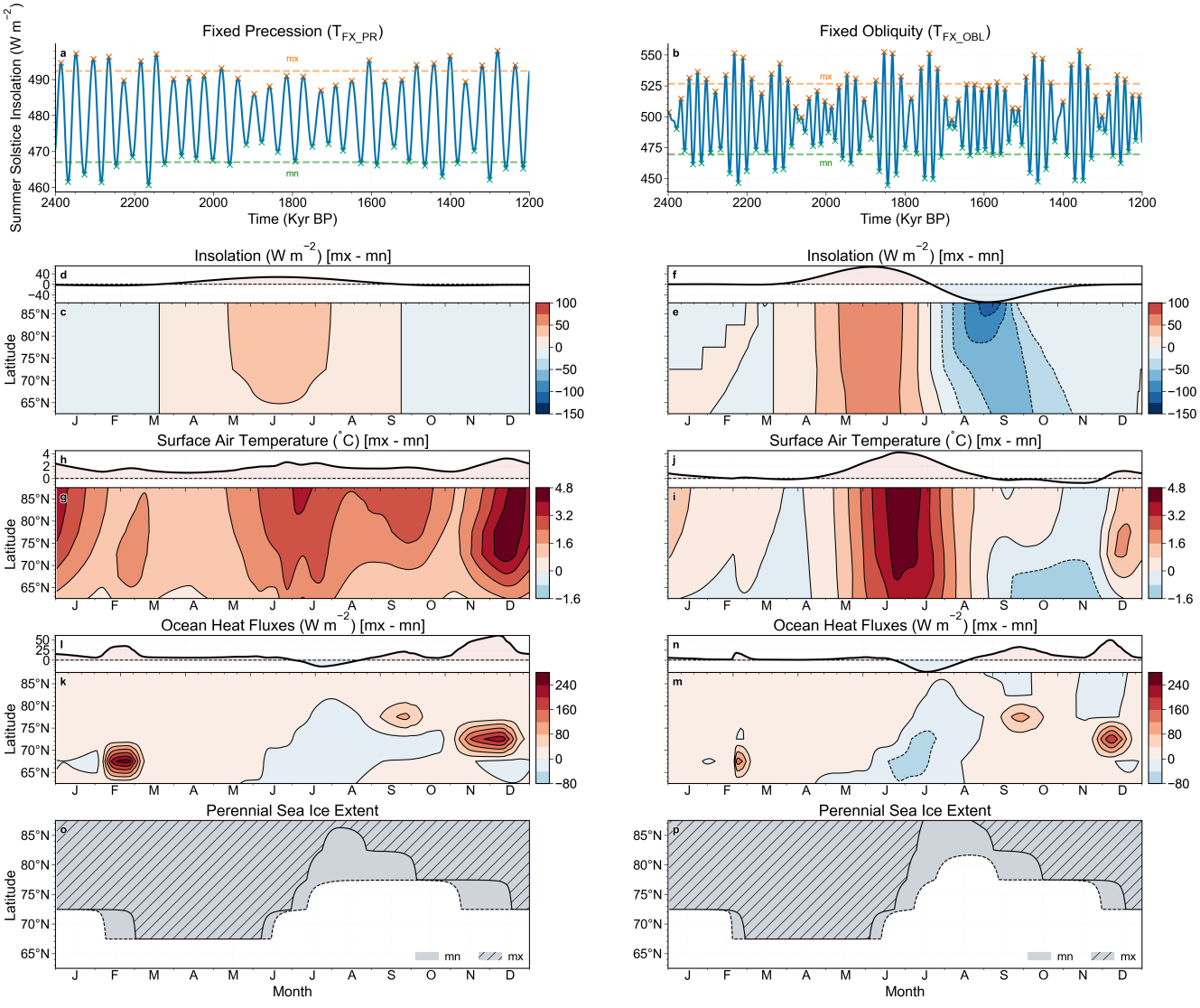

Figure 6. (a-b) Changes in summer solstice insolation (June 21st at 65°N) for the T_{FX_PR} (a) and T_{FX_OB} (b) experiment. Extremes in obliquity and precession are identified by maxima and minima in summer solstice insolation, shown with the orange and green crosses, respectively. Changes in insolation for extremes in obliquity (c-d) and precession (e-f), showing the seasonal cycle with latitude (c,e) and the average over the NH polar regions (d,f). As for insolation, we show changes in surface air temperature (g-j), upwards ocean heat fluxes including longwave radiation, sensible and latent heat fluxes (l-n). Also shown is extent of perennial sea ice cover for maxima and minima in obliquity (o) and precession (p).

averaged over these periods corresponding to maximum and minimum orbital forcing, which are subtracted from one another to reveal the seasonal differences for extremes in obliquity and precession.

https://doi.org/10.5194/egusphere-2026-1151
Preprint. Discussion started: 18 March 2026

Beginning with insolation, extremes in the Earth's obliquity results in positive anomalies during the summer months at the high northern latitudes (Fig 6c). When these anomalies are averaged across the NH polar regions, they can exceed 20 W m^{-2} in June (Fig 6d). In contrast, extremes in precession produce much larger differences in daily mean insolation (Fig 6e). Although the mid-summer insolation peak approaches 70 W m^{-2} over the NH polar regions (Fig 6f), these strong positive anomalies are offset by equally strong negative insolation anomalies from August to October. Therefore, despite precession generating far stronger summer insolation peaks, as compared to obliquity, it does not affect annual mean insolation received at any latitude.

The corresponding differences in surface air temperature between periods of high and low obliquity shows a persistent warming throughout the year (Fig 6g). Despite obliquity primarily affecting summer insolation, warming is most intense during the winter months due to sea ice loss, exceeding 3°C in December (Fig 6h). In contrast, the alignment of NH summers with the perihelion, relative to the aphelion, generates the strongest warming in the mid-summer, exceeding 4°C in June and July, with a smaller temperature maxima occurring during the mid-winter (Fig 6i-j). However, the temperature difference is insignificant during other parts of the year for extremes in precession.

For extremes in both obliquity and precession, winter maxima in surface air temperature coincide with significant pulses of OHFs (Fig 6k-l). OHFs represents the upward transfer of longwave radiation, sensible heat, and latent heat from the surface ocean to the atmosphere. These strong positive OHF anomalies are closely associated with reductions in perennial sea ice cover (Fig 6m-o). The role of sea ice in regulating OHFs is linked to the vertical temperature gradient between the surface ocean and the atmosphere. During winter, when sea ice fully covers a latitudinal zone, the sea ice overlying the surface ocean is typically colder than the atmospheric layer above, creating a temperature inversion that inhibits the release of ocean heat to the atmosphere. In the absence of perennial sea ice, however, the surface ocean remains warmer than the overlying atmosphere, allowing large amounts of ocean heat to be released into the atmospheric layer. Since extremes in obliquity result in a greater winter retreat of perennial sea ice as compared to precession, they lead to larger pulses of OHF, causing an intense winter warming.

The importance of obliquity in controlling winter sea ice extent, and consequently the magnitude of OHFs, is further highlighted in the T_{BE} experiment, where all orbital parameters are allowed to vary (Fig 7). While the extent of summer sea ice, averaged from June to August, shows strong variability at both the obliquity and precession frequencies, winter sea ice, averaged from December to February, predominantly fluctuates with the 41-kyr obliquity cycle (Fig 7a-b). Although variability in winter sea ice extent is significantly lower than during the summer months, it has a visibly larger impact on OHFs (Fig 7c-d). As a result, even though the annual mean extent of sea ice exhibits strong 21-kyr and 41-kyr cycles, changes in OHFs are primarily controlled by the 41-kyr obliquity cycle, owing to its dependence on winter sea ice. Indeed, the dominant 41-kyr cyclicity in winter sea ice extent (Fig 7c) and annual-mean OHFs and surface air temperature (Fig 7f) further underscore the importance of this mechanism in regulating orbital sensitivity over the NH polar regions of ZEMBA.

4.4 Fixed sea ice (T_{FX_SI}) and snow cover (T_{FX_SC}) simulations

Figure 8 displays the changes in temperature, sea ice and snow cover over the NH polar regions when snow cover (T_{FX_SC}), sea ice (T_{FX_SI}) or both (T_{FX_SIC}) are kept fixed to the seasonal cycle from the E_{PI} simulation. Firstly, the comparison of

https://doi.org/10.5194/egusphere-2026-1151
Preprint. Discussion started: 18 March 2026

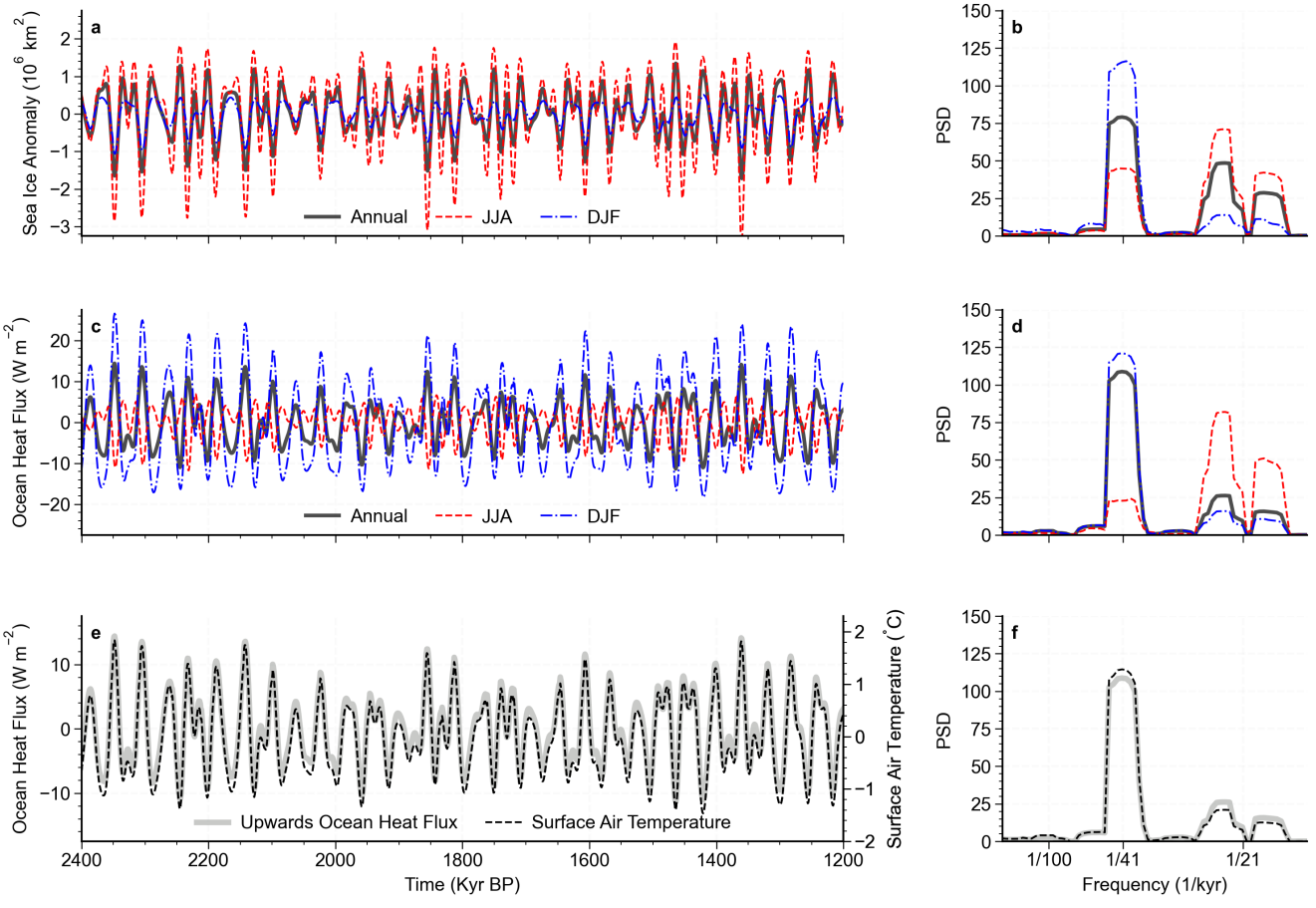

Figure 7. For the NH polar regions (60°-90°N): (top) variability in the annual mean (black lines), December-January-February (blue lines) and June-July-August (red lines) extent of sea ice, including the time-series (a) and the power spectral density of the time-series (b). (middle) the same as the top row but for changes in upwards surface ocean heat fluxes—comprising longwave radiation, sensible heat and latent heat. (bottom) Changes in annual mean OHFs (solid gray lines) a compared to annual mean surface air temperature (dashed black lines), in both the time-series (e) and the power spectral density (f).

https://doi.org/10.5194/egusphere-2026-1151
Preprint. Discussion started: 18 March 2026

annual mean surface air temperatures across all experiments demonstrates the importance of varying sea ice and snow cover for amplifying the response to changing orbital parameters in the polar regions of ZEMBA (Fig. 5a-b). The overall range of surface air temperature increases from 0.72° to 3.3° when sea ice and snow cover are allowed to vary. Moreover, temperature fluctuations are much larger for fixed snow cover, compared to fixed sea ice, which highlights the importance of sea ice in driving NH polar temperature variability. When only snow cover over land is allowed to vary (T_{FX_SI}), changes in surface air temperature are significantly diminished, with a variability that is virtually the same as when both sea ice and snow cover are fixed together. Moreover, sea ice appears very important in driving variability of snow cover over land (Fig. 5g-h). With fixed sea ice, the fluctuations in annual mean snow cover amount to 0.82 10^6 km^2, which more than doubles to 1.94 10^6 km^2 when sea ice is allowed to vary in tandem. Variations in sea ice and snow cover together are clearly important for generating the full variability in annual-mean surface air temperature (Fig. 5a-b), sea ice (Fig. 5d-e) and snow cover (Fig. 5g-h). Overall, these experiments involving fixed sea ice and snow cover demonstrates the key role of sea ice in driving temperature variability at the polar latitudes.

5 Discussion

Since the landmark findings from Hays et al. (1976) that benthic $\delta^{18}O$ proxies of ice volume and ocean temperature vary at the 23-, 41- and 100-kyr periodicities, in correspondence to changes in the Earth's orbital parameters, modeling studies have long attempted to understand the relationship between orbital forcing and climate change. To constrain the sensitivity of ZEMBA to orbital parameters, we first compared our model to climate models of similar complexity. Indeed, energy balance models (EBMs) were some of the first models to simulate the climate response to small variations in the Earth's orbit. First formulated by Budyko (1969) and Sellers (1969) independently, all physical processes in these seasonally-averaged models (i.e., pertaining to annual mean conditions) were parameterized in terms of surface temperature, and they were generally more sensitive to perturbations (i.e., to changes in the solar constant) compared to later and more complex iterations of climate models. However, these earliest versions of EBMs were found to be largely insensitive to changes in the Earth's orbit (Budyko, 1969; Coakley, 1979), especially at the polar latitudes (Sellers, 1970), which is perhaps unsurprising given their effect on annual mean insolation is much smaller relative to seasonal insolation anomalies. Yet even some of the first seasonal EBMs exhibited a muted sensitivity to extremes in obliquity and precession (North and Coakley, 1979), which has been attributed to highly simplified parameterizations for longwave radiation and snow cover (Held, 1982). Using a more complex EBM, similar in design to ZEMBA, Suarez and Held (1979) find a much larger sensitivity to changes in the Earth's orbit, with a simulation of the last 150 ka producing changes in NH mean temperature of up to 1.9°C, compared to 0.68°C for ZEMBA. However, their model is very sensitive to the solar constant ($\sim$ 4°C for a 1% change), and when the model was adjusted to reduce this sensitivity, the response of annual and global mean temperature to orbital perturbations was reported to be much smaller (Held, 1982). Overall, seasonal EBMs have produced varying sensitives to changes in the Earth's orbit, but with missing feedbacks in the climate system related to ice sheet dynamics, isostatic adjustments of the lithosphere, and CO_2—they do not reproduce the magnitude of temperature and snow/ice cover changes seen in proxy records of glacial-interglacial cycles. Later

https://doi.org/10.5194/egusphere-2026-1151
Preprint. Discussion started: 18 March 2026

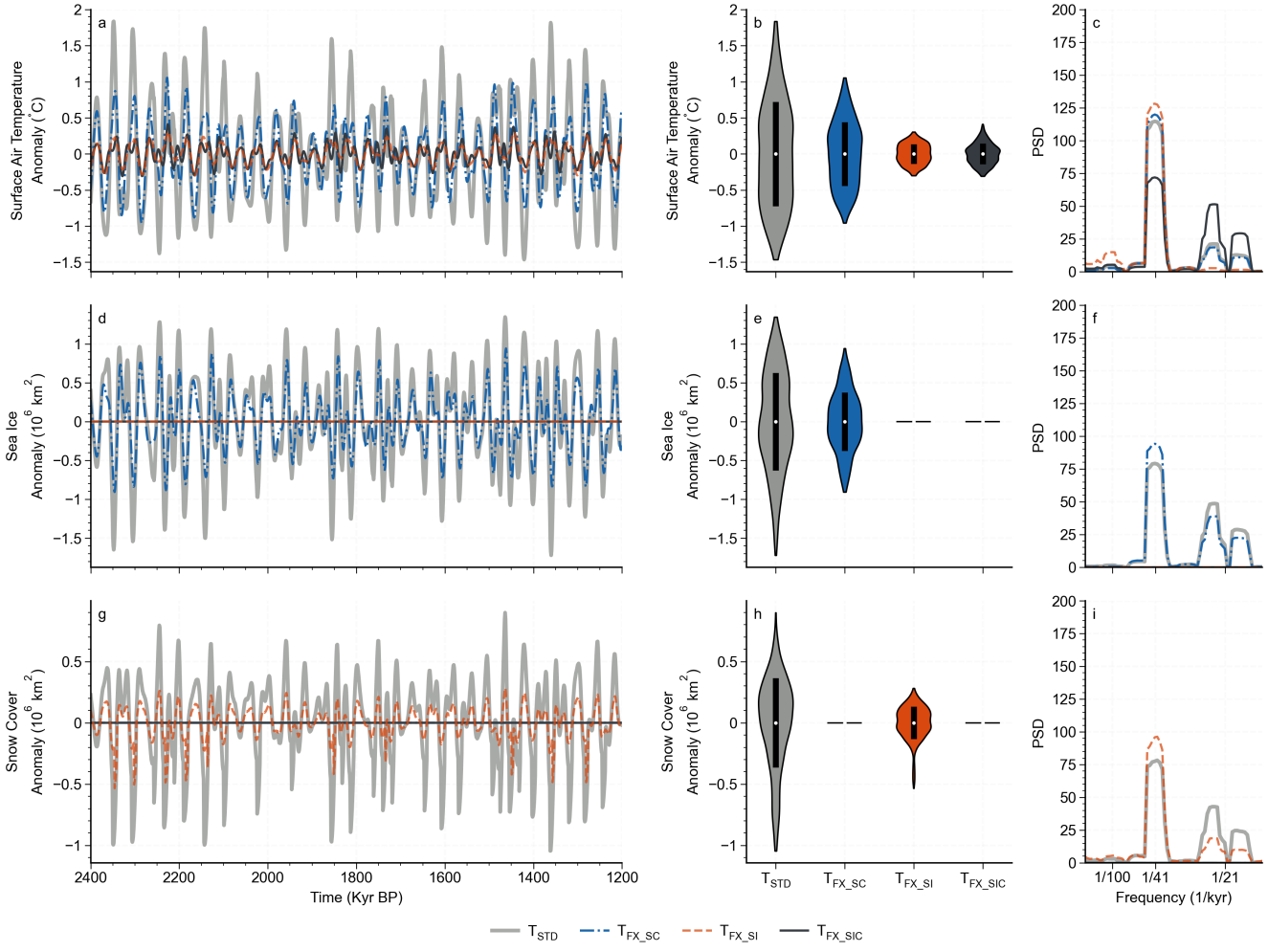

Figure 8. Same as Figure 5 but instead showing changes in surface air temperature (a-c), sea ice (d-f) and snow cover (g-i) over the NH polar regions (60°-90°N) for the standard T_{BE} (in grey), fixed snow cover T_{FX_SC} (in blue), fixed sea ice cover T_{FX_SI} (in orange) and fixed snow cover and sea ice cover T_{FX_SIC} (in black) experiments.

https://doi.org/10.5194/egusphere-2026-1151
Preprint. Discussion started: 18 March 2026

studies involving the coupling of EBMs to ice sheets produce larger-scale fluctuations in surface temperature, in addition to asymmetries more reflective of the proxy records (Pollard, 1982), which we intend to replicate in future studies with ZEMBA. For assessing the orbital sensitivity of ZEMBA without these longer timescale feedbacks, however, we can also compare ZEMBA to models of higher complexity employed to study the response of climate system to strong orbital forcing.

In a previous study (Gunning et al., 2025), we demonstrated that given a seasonal cycle in insolation, a CO_2 concentration and a percentage of land and ice sheet cover, ZEMBA could simulate both the PI and LGM climate in broad agreement to both observations and GCMs. Here, we find the sensitivity of ZEMBA to changes in the Earth's orbital parameters also broadly corresponds to climate models of higher complexity. In particular, the *lig127k* ensemble from PMIP4 enables the orbital sensitivity of ZEMBA to be compared to state-of-the-art climate models, in which the orbital parameters change but the other boundary conditions (i.e. ice sheet extent and CO_2) remains largely the same to the PI. We find the difference in zonal average and annual mean surface air temperature between the LIG and PI, driven solely by differences in the orbital configuration, is in good agreement between ZEMBA and the state-of-the-art climate models that contributed to the *lig127k* ensemble (Fig. 2c). In particular, ZEMBA reproduces the annual mean warming that occurs in the NH polar regions, driven by positive anomalies in summer insolation. Moreover, ZEMBA captures the reduction in Arctic sea ice extent (relative to PI) during the summer months, peaking around August-September (Fig. 2e), which is a consistent feature amongst models that contributed to *lig127k* (Otto-Bliesner et al., 2021; Kageyama et al., 2021). Focusing next on the transient sensitivity of the model to changing orbital parameters, the range of global mean temperature simulated by ZEMBA is 0.43°C. For comparison, a climate model of intermediate complexity (CLIMBER2) simulated a variability of 0.5°C when forced solely by changing orbital parameters, with fixed CO_2 and ice cover (Stap et al., 2018). Moreover, a suite of orbital sensitivity experiments were performed using the Hadley Centre Coupled Climate Model version 3 (HadCM3), maintaining a fixed ice sheet configuration and CO_2 concentration (Prescott et al., 2014). Focusing on natural climate variability for two interglacial periods within the Mid-Pliocene Warm Period (3.3 to 3.0 Ma), variations in the orbital parameters drove changes in global average temperature of up to 0.45°C (Prescott et al., 2014). Overall, we have confidence that ZEMBA simulates climate change induced by changing orbital parameters in accordance with climate models of higher complexity, thereby providing a useful tool for studying the sensitivity of climate to changes in obliquity and precession.

For the baseline simulation of ZEMBA (T_{BE}) in response to changing orbital parameters, the temperature range at the polar latitudes is 4.06 and 2.14°C for the NH and SH, respectively, varying predominantly at the 41-kyr obliquity cycle (Fig. 4a-b). We attribute the reduced variability in the southern high latitudes, relative to the north, to fixed ice sheet cover which encompasses the entire surface area of ZEMBA poleward of 75°S, thereby limiting surface albedo feedbacks. In contrast, changes in the annual-mean extent of sea ice and snow cover in the polar regions contains strong variance at both the precession and obliquity bands. The range of global mean temperature is 0.43°C and varies with both the 100-kyr eccentricity cycle and 41-kyr obliquity cycle (Fig. S2 in the Supplement). An increase in obliquity (i.e. more axial tilt) leads to more annual mean insolation and thereby warming at the polar latitudes, with less annual mean insolation and thereby cooling in the tropics (Fig. S3 in the Supplement). Due to the effect of eccentricity on global annual mean insolation, it also influences variability in global

https://doi.org/10.5194/egusphere-2026-1151
Preprint. Discussion started: 18 March 2026

annual mean temperature, which is most effective at the mid-latitudes where the affect of obliquity on annual mean insolation is lowest (Fig. S3 in the Supplement).

Changes in sea ice and snow cover are crucial for driving polar temperature variability in ZEMBA (Fig. 5). By performing the same transient simulation, but fixing both sea ice and snow cover (T_{FX_SIC}), the range of surface air temperature at the polar latitudes is reduced from 3.75°C to 0.73°C in the north, and 2.13°C to 0.68°C in the south. Sea ice, in particular, appears to be the main driver of temperature change, whereas snow cover by itself (i.e., with sea ice held constant) has a much smaller influence. In addition to the albedo feedback, the importance of sea ice is related to controlling the exchange of heat between the surface ocean and the atmospheric layer. For example, when sea ice covers a latitudinal band during the winter, the exchange of heat from the ocean to the atmosphere is restricted due to a temperature inversion. When sea ice retreats or decreases, however, the exposed ocean surface releases more heat into the atmosphere because there is no insulating ice layer to trap the heat, which contributes to more intense warming. These sensitivity experiments also demonstrate the importance of sea ice in driving snow cover variability over land (Fig. 8g). The necessity of sea ice is likely related to the release of ocean heat, together with ZEMBA adopting an 'infinite wind' mixing scenario. Following previous energy balance model studies (Peng et al., 1987; Bintanja, 1997), atmospheric temperature and humidity over land and ocean, but belonging to the same latitudinal band, is set equal to the zonal (i.e. land-ocean) average at the end of each model time-step. Therefore, this 'infinite wind' mixing scenario enables heat released by the ocean in regions of retreating sea ice to be instantaneously transferred over land, promoting melting of snow cover. While feedbacks related to sea ice and snow cover are important for polar temperature variability, they have a smaller influence on temperature changes at the lower and middle latitudes. For this reason, the range of global mean temperature is reduced to a lesser extent from 0.45 to 0.31°C when sea ice and snow cover are kept fixed.

A prominent feature of ZEMBA is the greater sensitivity of surface air temperatures to changes in the Earth's obliquity compared to precession. When all orbital parameters are varying (T_{BE}), the annual mean surface air temperature shows a dominant 41-kyr cycle in both the NH (Fig. 3a-b) and SH polar regions (Fig. S1 in the Supplement). Similarly, in the fixed orbital experiments, surface air temperature shows greater variability when ZEMBA is driven solely by changes in obliquity (T_{FX_PR}) than by precession (T_{FX_OB}) (Fig. 5a-b). Interestingly, the dominance of obliquity in surface air temperature cannot be explained by changes in the annual mean extent of sea ice or snow cover, as both obliquity and precession contribute significantly to the variability of these elements in the T_{BE} experiment. Moreover, the fixed orbit simulations (T_{FX_PR} and T_{FX_OB}) produce comparable variations in sea ice and snow cover. Given that surface albedo changes from sea ice and snow cover are a primary feedback mechanism in energy balance models like ZEMBA, the difference in periodicities between annual mean temperature, sea ice and snow cover is unexpected.

A closer inspection of the seasonal cycles in surface air temperature over the NH polar regions for the T_{FX_PR} and T_{FX_OB} experiments reveals that only changes in obliquity produces a sustained warming throughout the year, with maximum temperatures occurring in the winter months (Fig. 6). These pulses of winter warming align with reductions in perennial sea ice extent and large positive anomalies in OHFs. Although extremes in precession also generate winter maxima in surface air temperature due to sea ice retreat and associated OHFs, they are smaller in magnitude compared to obliquity. In the T_{BE} simulation, where all orbital parameters vary, precession strongly influences the summer and annual mean extent of sea ice, but winter sea

https://doi.org/10.5194/egusphere-2026-1151
Preprint. Discussion started: 18 March 2026

ice extent and annual mean OHFs follow a dominant 41-kyr cycle, consistent with surface air temperature patterns (Fig. 7). Therefore, the greater influence of obliquity on surface air temperatures in the NH polar regions can be attributed to its control on winter sea ice extent, which regulates heat exchange between the surface ocean and atmosphere.

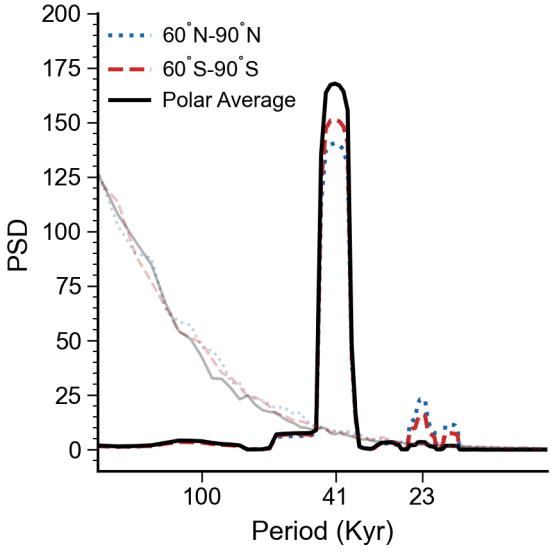

Figure 9. For the baseline T_{BE} experiment, with all orbital parameters varying, the power spectral density for changes in surface air temperature averaged in the NH polar regions (blue dotted line), SH polar regions (red dashed line) and the polar average across both hemispheres (black solid line). Thinner semi-transparent lines extending from the top left shows the corresponding 99% significance level for each time-series.

For extremes in precession, the increase in summer insolation when NH summer align with the perihelion instead of aphelion (Fig. 6e) causes an intense mid-summer warming (Fig. 6i). The annual mean warming that results from NH summers aligning with the perihelion demonstrates that feedbacks related to retreating sea ice and snow cover amplify the response to mid-summer insolation. However, the subsequent drop in insolation from August to October—due to Kepler's second law, which causes shorter summers when the Earth is closer to the Sun—restricts warming to the summer months and limits the retreat of winter sea ice, crucial for regulating OHFs (Fig. 7a-d). This counterbalancing between insolation intensity and summer duration reduces the impact of precession on surface air temperature, a phenomenon described as the "Achilles' heel of precession" (Huybers, 2006). In contrast, the more moderate increase in mid-summer insolation driven by extremes in obliquity leads to year-round warming (Fig. 6c-d), supported by a greater retreat of winter sea ice (Fig. 6l-k) and stronger OHFs (Fig. 6o). Indeed, Huybers (2006) argues that climate responds more to integrated summer insolation (ISI), which accounts for this balancing between summer insolation intensity and duration. We observe a strong correlation between ISI and polar temperature variability in both hemispheres (Fig. S5 and S6 in the Supplement), which aligns more closely with temperature trends than summer solstice insolation and slightly better than caloric summer half-year insolation.

https://doi.org/10.5194/egusphere-2026-1151
Preprint. Discussion started: 18 March 2026

While orbital simulations of ZEMBA allude to the importance of precession counterbalancing between insolation intensity and summertime duration (Huybers, 2006; Huybers and Tziperman, 2008) in explaining the dominance of obliquity, the pronounced 41-kyr cyclicity in surface air temperature is confined to the polar regions of ZEMBA. Without long-term climate feedbacks related to ice sheet dynamics and/or CO_2 variations, global mean temperature changes (of up to 0.43°C) are much smaller than those observed in proxy records and exhibit prominent 100-kyr cycles associated with the influence of eccentricity on annual global mean insolation. It remains uncertain whether the coupling ZEMBA to an ice sheet model will produce the same 41-kyr cyclicity at the polar regions and globally, a key goal for future research. Even without coupling to an ice sheet model, the 41-kyr cycles in polar surface air temperatures in ZEMBA are not as dominant as those observed in some benthic $\delta^{18}O$ records (Fig. 1a-b). Another mechanism proposed to account for the lack of strong precession cycles involves the cancellation out-of-phase precession between the NH ice sheets and Antarctica (Raymo et al., 2006). As a preliminary analysis, Figure 9 presents the power spectral density of surface air temperature changes in the NH polar regions, SH polar regions, and the polar average across both hemispheres. Both hemispheres show local 19- and 23-kyr precession cycles that largely cancel each other out when polar temperature variability is averaged across hemispheres, leaving behind a stronger obliquity cycle. Whether this relationship persists with ice sheet dynamics included needs to be examined in future studies.

6 Conclusions

In this study, we explore the sensitivity of a simplified climate model (ZEMBA) to variations in the Earth's orbital parameters, which are widely acknowledged to be the 'pacemaker' of the glacial-interglacial cycles during the Quaternary. By performing equilibrium simulations for the PI and the LIG, we asses how ZEMBA's orbital sensitivity compares to state-of-the-art climate models from the Coupled Model Intercomparison Project Phase 6 (CMIP6). Notably, the differences in surface air temperature correspond nicely between ZEMBA and the CMIP6 models, capturing the annual mean warming in the polar regions of the NH, driven by positive anomalies in summer insolation and reductions in Arctic sea ice extent. Given the primary goal of ZEMBA is to investigate climate sensitivity to changes in obliquity and climatic precession, the alignment of ZEMBA and CMIP6 models in terms of orbitally driven changes in temperature and sea ice is encouraging. Transient simulations of ZEMBA over the Early Pleistocene (2.4 to 1.2 Ma) reveal that temperature variability in polar regions is primarily associated with the 41-kyr obliquity cycle. Sensitivity experiments, where either sea ice or snow cover (over land) is held fixed, indicate that sea ice plays a crucial role in driving temperature changes at the higher latitudes. Additionally, fixed-orbit simulations show that obliquity exerts a stronger influence on surface air temperature in the NH due to its control over winter sea ice extent, which regulates the release of large stores of heat from the surface ocean to the atmosphere. These orbital simulations highlight the importance of a precession counterbalancing between insolation intensity and summertime duration, as shown in previous studies, for promoting strong 41-kyr obliquity cycles, but with added emphasis on the mechanism for limiting variability in sea ice extent and ocean heat fluxes during the winter months.

https://doi.org/10.5194/egusphere-2026-1151
Preprint. Discussion started: 18 March 2026

Code and data availability. Source code is maintained on GitHub at https://github.com/daniel-francis-james-gunning/zemba (last access: 25 Feb 2026) with the exact version used in this study (including scripts for creating all figures) archived on Zenodo at https://doi.org/10.5281/zenodo.18773155

Author contributions. DFJG designed and ran the model experiments. DFJG analysed the results and drafted the paper, with input from KHN, EC and RSWvdW.

Competing interests. The contact author has declared that none of the authors has any competing interests.

Acknowledgements. This publication was generated in the frame of DEEPICE project. The project has received funding from the European Union's Horizon 2020 research and innovation programme under the Marie Sklodowska-Curie grant agreement No 955750. Emilie Capron acknowledges the financial support from the French National Research Agency under the "Programme d'Investissements d'Avenir" (ANR-19-MPGA-0001). Kerim H. Nisancioglu acknowledges financial support from the ClimateNarratives project 324520 funded by the Research Council of Norway. We would like to thank Anni Zhao for providing files on the lig127k ensemble from PMIP4 that aided the assessment of ZEMBA's orbital sensitivity.

https://doi.org/10.5194/egusphere-2026-1151
Preprint. Discussion started: 18 March 2026

References

Abe-Ouchi, A., Saito, F., Kawamura, K., Raymo, M. E., Okuno, J., Takahashi, K., and Blatter, H.: Insolation-driven 100,000-year glacial cycles and hysteresis of ice-sheet volume, Nature, 500, 190–193, https://doi.org/10.1038/nature12374, 2013.

Ahn, S., Khider, D., Lisiecki, L. E., and Lawrence, C. E.: A probabilistic Pliocene–Pleistocene stack of benthic δ18O using a profile hidden Markov model, Dynamics and Statistics of the Climate System, 2, 1–16, https://doi.org/10.1093/climsys/dzx002, 2017.

Argus, D., Peltier, W., Drummond, R., and Moore, A.: The Antarctica component of postglacial rebound model ICE-6G_C (VM5a) based on GPS positioning, exposure age dating of ice thicknesses, and relative sea level histories, Geophysical Journal International, 198, 537–563, https://doi.org/10.1093/gji/ggu140, 2014.

Bereiter, B., Eggleston, S., Schmitt, J., Nehrbass-Ahles, C., Stocker, T. F., Fischer, H., Kipfstuhl, S., and Chappellaz, J.: Revision of the EPICA Dome C CO2 record from 800 to 600-kyr before present, Geophysical Research Letters, 42, 542–549, https://doi.org/10.1002/2014GL061957, 2015.

Berends, C. J., de Boer, B., and van de Wal, R. S. W.: Reconstructing the evolution of ice sheets, sea level, and atmospheric CO_2 during the past 3.6 million years, Climate of the Past, 17, 361–377, https://doi.org/10.5194/cp-17-361-2021, 2021.

Berger, A., Li, X. S., and Loutre, M. F.: Modelling northern hemisphere ice volume over the last 3 Ma, Quaternary Science Reviews, 18, 1–11, https://doi.org/10.1016/S0277-3791(98)00033-X, 1999.

Bintanja, R.: Sensitivity Experiments Performed with an Energy Balance Atmosphere Model Coupled to an Advection-diffusion Ocean Model, Theoretical and Applied Climatology, 56, 1–24, https://doi.org/10.1007/BF00863779, 1997.

Budyko, M. I.: The effect of solar radiation variations on the climate of the Earth, Tellus, 21, 611–619, https://doi.org/10.1111/j.2153-3490.1969.tb00466.x, 1969.

Clark, P. U., Archer, D., Pollard, D., Blum, J. D., Rial, J. A., Brovkin, V., Mix, A. C., Pisias, N. G., and Roy, M.: The middle Pleistocene transition: characteristics, mechanisms, and implications for long-term changes in atmospheric pCO2, Quaternary Science Reviews, 25, 3150–3184, https://doi.org/10.1016/j.quascirev.2006.07.008, 2006.

Coakley, J. A. J.: A Study of Climate Sensitivity Using a Simple Energy Balance Model, Journal of the Atmospheric Sciences, 36, 260–269, https://doi.org/10.1175/1520-0469(1979)036<0260:ASOCSU>2.0.CO;2, 1979.

Elderfield, H., Ferretti, P., Greaves, M., Crowhurst, S., McCave, I. N., Hodell, D., and Piotrowski, A. M.: Evolution of ocean temperature and ice volume through the mid-Pleistocene climate transition, Science, 337, 704–709, https://doi.org/10.1126/science.1221294, 2012.

Ganopolski, A. and Calov, R.: The role of orbital forcing, carbon dioxide and regolith in 100 kyr glacial cycles, Climate of the Past, 7, 1415–1425, https://doi.org/10.5194/cp-7-1415-2011, 2011.

Gunning, D. F. J., Nisancioglu, K. H., Capron, E., and van de Wal, R. S. W.: ZEMBA v1.0: an energy and moisture balance climate model to investigate Quaternary climate, Geoscientific Model Development, 18, 2479–2508, https://doi.org/10.5194/gmd-18-2479-2025, 2025.

Hays, J. D., Imbrie, J., and Shackleton, N. J.: Variations in the earth's orbit: Pacemaker of the ice ages, Science, 194, https://doi.org/10.1126/science.194.4270.1121, 1976.

Held, I. M.: Climate Models and the Astronomical Theory of the Ice Ages, ICARUS, 50, 449–461, https://doi.org/10.1016/0019-1035(82)90135-X, 1982.

Hobart, B., Lisiecki, L. E., Rand, D., Lee, T., and Lawrence, C. E.: Late Pleistocene 100-kyr glacial cycles paced by precession forcing of summer insolation, Nature Geoscience, 16, 717–722, https://doi.org/10.1038/s41561-023-01235-x, 2023.

https://doi.org/10.5194/egusphere-2026-1151
Preprint. Discussion started: 18 March 2026

Huybers, P.: Early Pleistocene Glacial Cycles and the Integrated Summer Insolation Forcing, Science, 313, 508–511, https://doi.org/10.1029/2004PA001071, 2006.

Huybers, P.: Combined obliquity and precession pacing of late Pleistocene deglaciations, Nature, 480, 229–232, https://doi.org/10.1038/nature10626, 2011.

Huybers, P. and Tziperman, E.: Integrated summer insolation forcing and 40,000-year glacial cycles: The perspective from an ice-sheet/energy-balance model, Paleoceanography, 23, https://doi.org/10.1029/2007PA001463, 2008.

Jouzel, J., Masson-Delmotte, V., Cattani, O., Dreyfus, G., Falourd, S., Hoffmann, G., Minster, B., Nouet, J., Barnola, J. M., Chappellaz, J., Fischer, H., Gallet, J. C., Johnsen, S., Leuenberger, M., Loulergue, L., Luethi, D., Oerter, H., Parrenin, F., Raisbeck, G., Raynaud, D., Schilt, A., Schwander, J., Selmo, E., Souchez, R., Spahni, R., Stauffer, B., Steffensen, J. P., Stenni, B., Stocker, T. F., Tison, J. L., Werner, M., and Wolff, E. W.: Orbital and Millennial Antarctic Climate Variability over the Past 800,000 Years, Science, 317, 793–796, https://doi.org/10.1126/science.1141038, 2007.

Kageyama, M., Sime, L. C., Sicard, M., Guarino, M. V., Vernal, A. D., Stein, R., Schroeder, D., Malmierca-Vallet, I., Abe-Ouchi, A., Bitz, C., Braconnot, P., Brady, E. C., Cao, J., Chamberlain, M. A., Feltham, D., Guo, C., Legrande, A. N., Lohmann, G., Meissner, K. J., Menviel, L., Morozova, P., Nisancioglu, K. H., Otto-Bliesner, B. L., O'Ishi, R., Buarque, S. R., Melia, D. S. Y., Sherriff-Tadano, S., Stroeve, J., Shi, X., Sun, B., Tomas, R. A., Volodin, E., Yeung, N. K., Zhang, Q., Zhang, Z., Zheng, W., and Ziehn, T.: A multi-model CMIP6-PMIP4 study of Arctic sea ice at 127 ka: Sea ice data compilation and model differences, Climate of the Past, 17, 37–62, https://doi.org/10.5194/cp-17-37-2021, 2021.

Khider, D., Emile-Geay, J., Zhu, F., James, A., Landers, J., Ratnakar, V., and Gil, Y.: Pyleoclim: Paleoclimate Timeseries Analysis and Visualization With Python, Paleoceanography and Paleoclimatology, 37, https://doi.org/10.1029/2022PA004509, 2022.

Laskar, J., Robutel, P., Joutel, F., Gastineau, M., Correia, A. C., and Levrard, B.: A long-term numerical solution for the insolation quantities of the Earth, Astronomy and Astrophysics, 428, 261–285, https://doi.org/10.1051/0004-6361:20041335, 2004.

Lisiecki, L. and Raymo, M.: Pliocene-Pleistocene stack of globally distributed benthic stable oxygen isotope records., Paleoceanography., 20, https://doi.org/10.1029/2004PA001071, 2005.

Morée, A. L., Sun, T., Bretones, A., Straume, E. O., Nisancioglu, K., and Gebbie, G.: Cancellation of the Precessional Cycle in δ18O Records During the Early Pleistocene, Geophysical Research Letters, 48, https://doi.org/10.1029/2020GL090035, 2021.

North, G. R. and Coakley, J. A. J.: Differences between Seasonal and Mean Annual Energy Balance Model Calculations of Climate and Climate Sensitivity, Journal of the Atmospheric Sciences, 36, 1189–1204, https://doi.org/10.1175/1520-0469(1979)036<1189:DBSAMA>2.0.CO;2, 1979.

Otto-Bliesner, B. L., Braconnot, P., Harrison, S. P., Lunt, D. J., Abe-Ouchi, A., Albani, S., Bartlein, P. J., Capron, E., Carlson, A. E., Dutton, A., Fischer, H., Goelzer, H., Govin, A., Haywood, A., Joos, F., Legrande, A. N., Lipscomb, W. H., Lohmann, G., Mahowald, N., Nehrbass-Ahles, C., Pausata, F. S., Peterschmitt, J. Y., Phipps, S. J., Renssen, H., and Zhang, Q.: The PMIP4 contribution to CMIP6 - Part 2: Two interglacials, scientific objective and experimental design for Holocene and Last Interglacial simulations, Geoscientific Model Development, 10, 3979–4003, https://doi.org/10.5194/gmd-10-3979-2017, 2017.

Otto-Bliesner, B. L., Brady, E. C., Zhao, A., Brierley, C. M., Axford, Y., Capron, E., Govin, A., Hoffman, J. S., Isaacs, E., Kageyama, M., Scussolini, P., Tzedakis, P. C., Williams, C. J., Wolff, E., Abe-Ouchi, A., Braconnot, P., Buarque, S. R., Cao, J., Vernal, A. D., Guarino, M. V., Guo, C., Legrande, A. N., Lohmann, G., Meissner, K. J., Menviel, L., Morozova, P. A., Nisancioglu, K. H., O'Ishi, R., Mélia, D. S. Y., Shi, X., Sicard, M., Sime, L., Stepanek, C., Tomas, R., Volodin, E., Yeung, N. K., Zhang, Q., Zhang, Z., and Zheng, W.: Large-scale features of Last Interglacial climate: Results from evaluating the lig127k simulations for the Coupled Model Intercomparison Project

https://doi.org/10.5194/egusphere-2026-1151
Preprint. Discussion started: 18 March 2026

(CMIP6)-Paleoclimate Modeling Intercomparison Project (PMIP4), Climate of the Past, 17, 63–94, https://doi.org/10.5194/cp-17-63-2021, 2021.

Parrenin, F. and Paillard, D.: Terminations VI and VIII (∼ 530 and ∼ 720 kyr BP) tell us the importance of obliquity and precession in the triggering of deglaciations, Climate of the Past, 8, 2031–2037, https://doi.org/10.5194/cp-8-2031-2012, 2012.

Peltier, W. R., Argus, D. F., and Drummond, R.: Space geodesy constrains ice age terminal deglaciation: The global ICE-6G-C (VM5a) model, Journal of Geophysical Research: Solid Earth, 120, 450–487, https://doi.org/10.1002/2014JB011176, 2014.

Peng, L., Chou, M. D., and Arking, A.: Climate warming due to increasing atmospheric CO2: Simulations with a multilayer coupled atmosphere-ocean seasonal energy balance model, Journal of Geophysical Research, 92, 5505–5521, https://doi.org/10.1029/JD092iD05p05505, 1987.

Pollard, D.: A simple ice sheet model yields realistic 100 kyr glacial cycles, Nature, 296, 334–338, https://doi.org/10.1038/296334a0, 1982.

Prescott, C. L., Haywood, A. M., Dolan, A. M., Hunter, S. J., Pope, J. O., and Pickering, S. J.: Assessing orbitally-forced interglacial climate variability during the mid-Pliocene Warm Period, Earth and Planetary Science Letters, 400, 261–271, https://doi.org/10.1016/j.epsl.2014.05.030, 2014.

Raymo, M. E. and Nisancioglu, K.: The 41 kyr world: Milankovitch's other unsolved mystery, Paleoceanography, 18, https://doi.org/10.1029/2002pa000791, 2003.

Raymo, M. E., Lisiecki, L. E., and Nisancioglu, K. H.: Plio-Pleistocene Ice Volume, Antarctic Climate, and the Global d18O Record, Science, 313, 492–495, https://doi.org/10.1126/science.1123296, 2006.

Rohling, E. J., Foster, G. L., Grant, K. M., Marino, G., Roberts, A. P., Tamisiea, M. E., and Williams, F.: Sea-level and deep-sea-temperature variability over the past 5.3 million years, Nature, 508, 477–482, https://doi.org/10.1038/nature13230, 2014.

Sellers, W. D.: A Global Climatic Model Based on the Energy Balance of the Earth-Atmosphere System, Journal of Applied Meteorology, 8, 392–400, https://doi.org/10.1175/1520-0450(1969)008<0392:AGCMBO>2.0.CO;2, 1969.

Sellers, W. D.: The Effect of Changes in the Earth's Obliquity on the Distribution of Mean Annual Sea-Level Temperatures, Journal of Applied Meteorology, 9, 960–961, https://doi.org/10.1175/1520-0450(1970)009<0960:TEOCIT>2.0.CO;2, 1970.

Stap, L. B., van de Wal, R. S. W., de Boer, B., Köhler, P., Hoencamp, J. H., Lohmann, G., Tuenter, E., and Lourens, L. J.: Modeled Influence of Land Ice and CO2 on Polar Amplification and Paleoclimate Sensitivity During the Past 5 Million Years, Paleoceanography and Paleoclimatology, 33, 381–394, https://doi.org/10.1002/2017PA003313, 2018.

Suarez, M. J. and Held, I. M.: The sensitivity of an energy balance climate model to variations in the orbital parameters., Journal of Geophysical Research, 84, 4825–4836, https://doi.org/10.1029/jc084ic08p04825, 1979.

Tzedakis, C., Crucifix, M., Mitsui, T., and Wolff, E.: A simple rule to determine which insolation cycles lead to interglacials, Nature, 542, 427–432, https://doi.org/10.1038/nature21364, 2017.

Watanabe, Y., Abe-Ouchi, A., Saito, F., Kino, K., O'ishi, R., Ito, T., Kawamura, K., and Chan, W. L.: Astronomical forcing shaped the timing of early Pleistocene glacial cycles, Communications Earth and Environment, 4, https://doi.org/10.1038/s43247-023-00765-x, 2023.

Willeit, M., Ganopolski, A., Calov, R., and Brovkin, V.: Mid-Pleistocene transition in glacial cycles explained by declining CO2 and regolith removal, Science Advances, 5, https://doi.org/10.1126/sciadv.aav7337, 2019.